Biological Cybernetics (2019) 113:347–356
https://doi.org/10.1007/s00422-019-00799-5

Biological Cybernetics

ORIGINAL ARTICLE

Modeling of spike trains in auditory nerves with self-exciting point processes of the von Mises type

Hiroyuki Mino[1]

Received: 25 June 2018 / Accepted: 8 April 2019 / Published online: 19 April 2019

Abstract
This article presents the modeling of spike trains in auditory nerve fiber (ANF) models with a one-memory self-exciting point process (SEPP) of the von Mises type. The ANF models were acoustically stimulated by a synaptic current of inner hair cells, or electrically stimulated by sinusoidally amplitude-modulated pulsatile waveforms. It has been shown that the parameters of one-memory SEPP of the von Mises type could be estimated by numerically maximizing the likelihood function from sample realizations of the spike trains in response to acoustic or electric stimulus. Furthermore, it was found that period histograms of the one-memory SEPP generated artificially on the basis of the estimated von Mises parameters agreed well with those of acoustic or electric stimulus, by performing the uniform-scores test. It implies that the waveforms of pulsatile electric stimuli should be selected such that the spike trains can be represented by one-memory SEPP of the von Mises type with appropriate parameters, efficiently carrying information to the cochlear implant user's brain, like that in acoustic stimulation of the healthy ear. The findings presented in this paper may play an important role in determining optimal parameters of pulsatile electric stimuli by using one-memory SEPP of the von Mises type, and further in the design of better cochlear prostheses.

Keywords Self-exciting point process · Directional statistics · Maximum likelihood estimation · Monte Carlo simulations · Auditory neural prosthesis

1 Introduction

Random phenomena with a background of periodicity have been represented by a circular normal distribution, a von Mises distribution, as directional or circular statistics (Mardia and Jupp 1999). The von Mises distribution has been extensively applied to specifying some phenomena observed in natural sciences such as bird migration (Mouritsen and Ritz 2005), wind direction (Carta et al. 2008), and neural responses (Goldberg and Brown 1969). In auditory neurophysiology, neural spike trains in response to acoustic stimulation have been modeled as an inhomogeneous Poisson process with an intensity function being expressed as a periodic function with von Mises distribution, (Siebert and Gray 1963; Siebert 1965, 1970; Colburn et al. 2003; Heinz et al. 2001; Ashida et al. 2010; van Hemmen et al. 2011; van Hemmen 2013).

A neuron inherently has "dead time" immediately after a spike fires, a refractory period, which prevents the neuron from generating spike firings even when the stimuli are suprathreshold (Gray 1967; Gaumond et al. 1982, 1983; Bi 1989; Li and Young 1993). The refractory periods may affect information transmission between neurons more or less (Berry and Meister 1998; Mino and Rubinstein 2006). Random point processes with a history of the previous point occurrences are self-exciting point processes (Hawkes 1971a, b; Ozaki 1979; Ogata 1981, 1983; Ogata et al. 1982; Ogata and Katsura 1986; Snyder and Miller 1991; Daley and Vere-Jones 2003). A one-memory self-exciting point process (SEPP) has been proposed as a strong candidate to model auditory neural spike trains in response to acoustic stimulation (Johnson and Swami 1983; Miller 1985; Mark and Miller 1992), since a one-memory SEPP can account for aftereffects with a history of the latest spike occurrences (Mino 2001).

However, it is yet unclear whether or not electrically stimulated auditory nerves can be represented by a one-memory SEPP with an intensity process being expressed as a periodic

Communicated by Benjamin Lindner.

✉ Hiroyuki Mino
mino@ieee.org

[1] Department of Electrical Engineering, Kanto Gakuin University, 1-50-1 Mutsuura E., Kanazawa-ku, Yokohama 236-8501, Japan

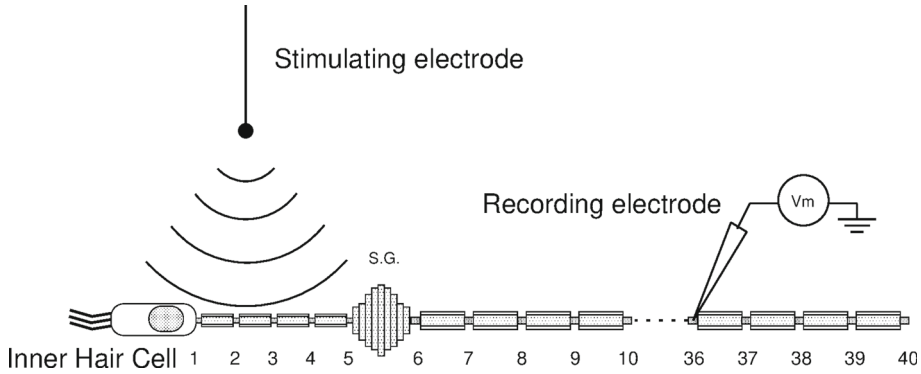

Fig. 1 The ANF model has 40 nodes of Ranvier and consists of 400 compartments. S.G. denotes a spiral ganglion cell with a diameter of 27 μm in the center. As a bipolar cell, the axons of the peripheral side and the central side are connected to inner hair cell and cochlear nuclei in the brain stem, respectively. A stimulating electrode is located at a distance of 1 mm above the second node of Ranvier, while the transmembrane potentials are recorded at the 36th node of Ranvier. Note that length is not to scale. [Adopted and modified from Mino et al. (2004), Mino (2007) and Kumsa and Mino (2012)]

function of von Mises distribution in addition to refractoriness, although some studies regarding a point process framework have been reported (Goldwyn et al. 2010; Mino 2016).

The objective of this article was twofold: (i) to investigate whether or not the spike trains of the auditory nerve fiber model consisting of stochastic node of Ranvier in response to acoustic stimuli at inner hair cell, or pulsatile electric stimuli, can be represented by a one-memory SEPP of the von Mises type, i.e., to see if the parameters of a von Mises distribution can be estimated on the basis of the maximum likelihood principle from observation of the sample realizations of the spike trains, where the parameters of refractoriness were assumed to be known; (ii) to assess the validity of designing an optimal electric stimulating waveform determined in terms of matching the von Mises parameters between acoustic and electric stimuli via a one-memory SEPP of the von Mises type, by performing a statistical test of the equality of two distributions, the uniform-scores test. The purpose of seeking "optimal" electric stimulus is to improve hearing performances for cochlear implant users.

This paper is organized as follows: Methods are described in Sect. 2, and Results are shown in Sect. 3, followed by Discussion and Conclusion in Sect. 4.

2 Methods

2.1 Auditory nerve model

The auditory nerve fiber (ANF) model was composed of spiral ganglion and 40 sections of the node and myelin sheath and was represented by the multi-compartment model of 400 compartments (McNeal 1976; Colombo and Parkins 1987; Finley et al. 1990; Frijns et al. 1994; Matsuoka et al. 2001) as shown in Fig. 1, (Mino et al. 2004; Cartee 2006; Kumsa and Mino 2012). In the peripheral side, the diameter of the node of Ranvier and the width of the node gap were set at 1.2 μm and 1.0 μm, while the diameter of the myelin and the length of the long axis of the myelin part were set at 2.0 μm and 184 μm. In the central side, the diameter of the node of Ranvier and the width of the node gap were set at 1.5 μm and 1.0 μm, whereas the diameter of the myelin and the length of the long axis of the myelin were set at 2.5 μm and 230 μm. The diameter of spiral ganglion was set at 27 μm. Figure 1 depicts an ANF model with an inner hair cell as well as a stimulating electrode. In the cable model, the stochastic sodium and potassium channel models (Clay and DeFelice 1983; Rubinstein 1995) were incorporated into each node of Ranvier, in which 180 sodium and 100 potassium channels were modeled by a discrete-state Markov process (Neher and Stevens 1977; Papoulis 1985) with eight and five states, respectively, and were implemented by the channel number tracking algorithm (Mino et al. 2002). The other parameters, including resistance, capacitance, ion conductance, resting, and equilibrium potential in fibers, were adopted from those in (Mino et al. 2004; Cartee 2006; Mino 2007).

The transmembrane potentials can be expressed as a function of space k and time t and were solved numerically by the following equations (Mino et al. 2004):

$$\begin{aligned}&\frac{V_m^{[k+1]}(t)-V_m^{[k]}(t)}{R_a^{[k+1,k]}}-\frac{V_m^{[k]}(t)-V_m^{[k-1]}(t)}{R_a^{[k,k-1]}}\\&+\frac{V_e^{[k+1]}(t)-V_e^{[k]}(t)}{R_a^{[k+1,k]}}-\frac{V_e^{[k]}(t)-V_e^{[k-1]}(t)}{R_a^{[k,k-1]}}\\&=C_m^{[k]}\frac{V_m^{[k]}(t+\Delta t)-V_m^{[k]}(t)}{\Delta t}+\frac{V_m^{[k]}(t)}{R_m^{[k]}}+I_{\text{ion}}^{[k]}(t)\end{aligned}\quad(1)$$

where

$$V_e^{[k]}(t) = \frac{\rho}{4\pi z_d} I_{\mathrm{ele}}(t) \tag{2}$$

where $V_e^{[k]}(t)$, $(k = 1, 2, \ldots, 400)$, ρ, z_d, and $I_{\mathrm{ele}}(t)$ denote the extracellular potentials, the extracellular resistivity, the distance from a stimulating electrode, and the electric stimulating current, respectively, and where

$$I_{\mathrm{ion}}^{[k]}(t) = \begin{cases} \gamma_{\mathrm{Na}} N_{\mathrm{Na}}^{[k]}(t)(V_m^{[k]}(t) - E_{\mathrm{Na}}) \\ \quad + \gamma_{\mathrm{k}} N_{\mathrm{K}}^{[k]}(t)(V_m^{[k]}(t) - E_{\mathrm{K}}) + I_{\mathrm{ihc}}(t) \\ \qquad\qquad (\text{at } k = 1) \\ \gamma_{\mathrm{Na}} N_{Na}^{[k]}(t)(V_m^{[k]}(t) - E_{\mathrm{Na}}) \\ \quad + \gamma_{\mathrm{k}} N_{\mathrm{K}}^{[k]}(t)(V_m^{[k]}(t) - E_{\mathrm{K}}) \\ \qquad (\text{at node, exept 1st one}) \\ 0 \qquad\qquad (\text{otherwise}) \end{cases} \tag{3}$$

where $I_{\mathrm{ion}}^{[k]}(t)$, the ion channel current, $N_{\mathrm{Na}}^{[k]}(t)$ and $N_{\mathrm{K}}^{[k]}(t)$, the number of open channels in sodium and potassium channels that are expressed as a function of space k and time t, and $I_{\mathrm{ihc}}(t)$, the synaptic current of inner hair cell as a function of time t. γ_{Na} and γ_{k} denote the conductance of sodium and potassium channels, whereas E_{Na} and E_{K} stand for the reversal potential of sodium and potassium channels. The parameters of resistance, capacitance, conductance, and reversal potentials were adopted from those in (Mino 2007). In computer simulations, the transmembrane potentials $V_m^{[k]}(t)$ were solved numerically by the Crank–Nicholson method (Press et al. 1993) at a sampling step (Δt) of 2 μs.

2.2 Stimulus presentation and spike detection

The acoustic stimulating current, $I_{\mathrm{ihc}}(t)$, at inner hair cell synapse, was presented to the first node of Ranvier of the peripheral end. $I_{\mathrm{ihc}}(t)$ was expressed as a filtered inhomogeneous Poisson process (Snyder and Miller 1991):

$$I_{\mathrm{ihc}}(t) = \int_{-\infty}^{t} I_{\mathrm{amp}} e^{-(t-\tau)/\tau_{\mathrm{ihc}}} \mathrm{d}N_{\mathrm{ihc}}(\tau) \tag{4}$$

where $\tau_{\mathrm{ihc}} = 0.3$ ms, and $I_{\mathrm{amp}} = 3, 3.5, 4.0$, or 4.5 pA. $N_{\mathrm{ihc}}(t)$ stands for the counting process of the inhomogeneous Poisson process with the intensity function of inner hair cell activity:

$$\lambda_{\mathrm{ihc}}(t) = \lambda_{\mathrm{spon}} + \lambda_{\mathrm{sin}}(t) \tag{5}$$

$$\lambda_{\mathrm{sin}}(t) = \begin{cases} \lambda_{\mathrm{c}} \cos(2\pi f t) & (\lambda_{\mathrm{sin}}(t) > 0) \\ 0 & (\text{otherwise}) \end{cases} \tag{6}$$

where $f = 220, 440$, or 880 Hz, $\lambda_{\mathrm{spon}} = 50\,\mathrm{s}^{-1}$, $\lambda_{\mathrm{c}} = 1000, 1500, 2000, 2500$, or $3000\,\mathrm{s}^{-1}$, associated with inner hair cell activity, i.e., sound pressure level. Note that the acoustic stimulation presented above does not take a transient adaptation of inner hair cell synapse into account, as spike trains in response to sustained stimuli are considered. In our model, we consider a short time window in which wide-sense stationarity can be assumed. The assumption of stationarity has been extensively accepted in speech processing and recognition.

The stimulating electrode was located at a distance of 1 mm above the second node of Ranvier. The stimulating current presented to the electrode was an amplitude-modulated pulsatile waveform, since it has been adopted for cochlear implants in clinical situations (Tejani et al. 2017; McDermott 2004).

The stimulating current, $I_{\mathrm{ele}}(t)$, was expressed as:

$$I_{\mathrm{ele}}(t) = I_{\mathrm{pulse}}(t) \left\{ 1 + \frac{m}{100} \sin(2\pi f t + \Phi) \right\} \tag{7}$$

where f stands for a sinusoidal frequency of 220, 440, or 880 Hz, Φ denotes a randomized initial phase taking a value between 0 and 2π, and m designates a modulation depth set at 8, 10, 12, 14, 16, 18, 20, 22, or 24 %. The different kinds of sinusoidal frequency would be supposed to be different stimulating electrode of frequency bands, investigating frequency characteristics. $I_{\mathrm{pulse}}(t)$ denotes the unmodulated biphasic pulsatile waveform:

$$I_{\mathrm{pulse}}(t) = \begin{cases} I_{\mathrm{p}} \sum_{n=0} \{u(t - n\tau_{\mathrm{int}}) - 2u(t - w - n\tau_{\mathrm{int}}) \\ \quad + u(t - 2w - n\tau_{\mathrm{int}})\} \\ \quad (n\tau_{\mathrm{int}} \le t < n\tau_{\mathrm{int}} + 2w) \\ 0 \quad (\text{otherwise}) \end{cases} \tag{8}$$

where I_{p} denotes the amplitude of pulsatile stimuli at 260, 265, or 270 μA, $w = 40$ μs, and $\tau_{\mathrm{int}} = 0.2$ ms (5000 Hz), and in which $u(t)$ denotes a unit step function as follows:

$$u(t) = \begin{cases} 1 & (0 \le t) \\ 0 & (\text{otherwise}) \end{cases} \tag{9}$$

The spike firing time was detected by determining when the transmembrane potential showed the peak amplitude and was greater than 50% of the peak amplitude of typical action potentials. The post-stimulus time (PST) histogram and period histogram were generated from the spike trains in response to the stimulating current presented repeatedly 300 times.

2.3 One-memory SEPP of von Mises type

The characteristics of neural refractoriness can be incorporated into the intensity process of one-memory SEPPs as an event history H:

$$\lambda(t) = \lim_{\Delta \to 0} \frac{Pr[N[t, t+\Delta) = 1|H]}{\Delta} = X \exp(\kappa \cos(2\pi f t + \mu)) h(t - w_{N(t)}) \quad (10)$$

where $N(t)$ denotes the counting process, f denotes sinusoidal frequency, κ, and μ are the parameters of von Mises distribution, X stands for the parameter relating to the firing rate, and $w_i (i = 1, 2, \ldots, N(T))$ denotes the spike firing times and where

$$h(t) = \left(1 - e^{-\frac{t-\tau_{\text{abs}}}{\tau_{\text{ref}}}}\right) \quad (11)$$

in which τ_{abs} denotes the absolute refractory period at 0.3 ms, while τ_{ref} denotes the relative refractory period at 0.5 ms (Mino and Rubinstein 2006).

The log-likelihood function of one-memory SEPPs is expressed as (Snyder and Miller 1991):

$$\begin{aligned} L(N(t)|\theta) &= -\int_0^T \lambda(\sigma) \mathrm{d}\sigma + \int_0^T \ln[\lambda(\sigma)] \mathrm{d}N(\sigma) \\ &= -X \int_0^{\mathrm{T}} e^{\kappa \cos(2\pi f \sigma + \mu)} h(t - w_{N(\sigma)}) \mathrm{d}\sigma \\ &\quad + \int_0^T \ln[X e^{\kappa \cos(2\pi f \sigma + \mu)} h(t - w_{N(\sigma)})] \mathrm{d}N(\sigma) \end{aligned} \quad (12)$$

where $\theta = [X\ \kappa\ \mu]^{\mathrm{T}}$ denotes the parameters of the von Mises distribution. The maximum likelihood parameter estimation needs to be solved by computationally or numerically maximizing the log-likelihood function with the simplex method (Press et al. 1993).

In practical situations, the number of sample realizations P was set at 10, so that the parameter θ was estimated using the data from 2 s of recording time, as T was set at 200 ms. For P stimulus presentations, the log-likelihood function should be replaced by

$$\begin{aligned} L^{(P)}(N(t)|\theta) &= -\sum_{p=1}^{P} X \int_0^T e^{\kappa \cos(2\pi f \sigma + \mu)} h(t - w_{N(\sigma)}^{(p)}) \mathrm{d}\sigma \\ &\quad + \sum_{p=1}^{P} \int_0^T \ln\left[X e^{\kappa \cos(2\pi f \sigma + \mu)} h \right. \\ &\quad \left. \left(t - w_{N(\sigma)}^{(p)}\right)\right] \mathrm{d}N(\sigma) \end{aligned} \quad (13)$$

We note that the intensity function (sample function) is one of the stochastic processes, and thus the intensity "process", as seen from the fact that the function $h(t)$ of event history is generated from the spike occurrence times, $w_i^{(p)}$ (see Fig. 2).

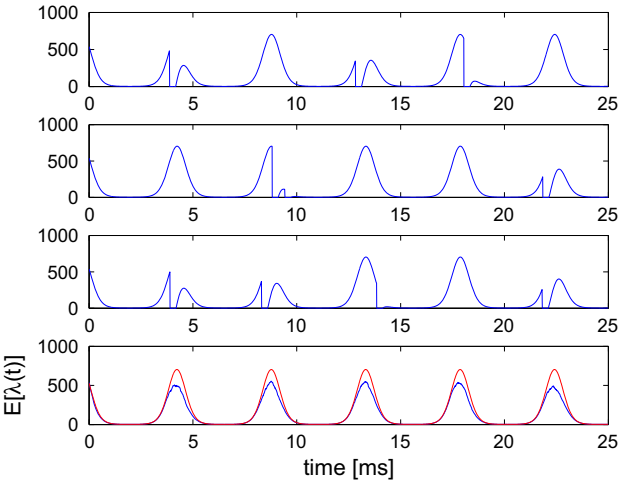

Fig. 2 Three typical sample realizations of the intensity processes in one-memory SEPP of the von Mises type in which $X = 35.0$, $\kappa = 3.0$, $\mu = 0.424$, $f = 220$ Hz, (1–3 rows); the expected value (mean) of the intensity processes (blue), in addition to superimposed von Mises function without aftereffects of refractoriness $X \exp(\kappa \cos(2\pi f t + \mu))$ (red) (bottom row). Note that in 1–3 rows it follows from the function $h(t)$ of history that at each spike firing occurrence time the intensity takes a value of zero and recovers exponentially with time, and that each intensity process is quite different from others depending on the spike firing occurrence time. Note also that in the bottom trace the expected value (blue) could be decreased due to distortions by refractoriness in a comparison with the trace of von Mises function (red) (color figure online)

In the present paper, the firing rates, f_{spike}, and vector strength, VS, were calculated by substituting the estimated von Mises parameters of SEPPs, $\hat{X}$ and $\hat{\kappa}$, into the expressions described below in Eqs. (14) and (15). Equations (14) and (15) came from the expressions of the maximum likelihood estimates in which the neural spike trains could be represented by the IHPP of the von Mises type without refractory components (Siebert and Gray 1963; Siebert 1965; Snyder and Miller 1991):

$$f_{\text{spike}} = \hat{X} I_0(\hat{\kappa}) \quad (14)$$

$$\text{VS} = I_1(\hat{\kappa}) / I_0(\hat{\kappa}) \quad (15)$$

where $I_0()$ and $I_1()$ stand for the modified Bessel function of the first kind of order 0 and 1. We note that the expressions of (14) and (15) would indicate the statistics corrected for removing neuron's refractory component via SEPP modeling.

2.4 The uniform-scores test

The uniform-scores test (Mardia and Jupp 1999) was carried out to determine whether or not the period histogram of the spike trains in response to acoustic or electric stimulus could be close to that of artificially generated one-memory SEPPs of the von Mises type, i.e., to test the equality of

two distributions of the period histograms. The uniform-scores test is a nonparametric test and would look like a Kolmogorov–Smirnov test for directional statistics. The null hypothesis in our case was expressed as follows: "$H_0 : F_1 = F_2$, against $H_1 : F_1 \neq F_2$" where F_1 and F_2 denote the distribution functions of the period histograms, on the basis of angle data $[\theta_{11}, \theta_{12}, \ldots, \theta_{1N_1}]$ and $[\theta_{21}, \theta_{22}, \ldots, \theta_{1N_2}]$, $(0 \leq \theta_{xx} < 2\pi)$, sampled and transferred from the spike firing times of acoustically or electrically stimulated auditory nerve models (group 1) and the artificially generated SEPP model of the von Mises type (group 2), where N_1 and N_2 denote the number of angle data. The period histograms were generated from these angle data. Furthermore, the equality of two period histograms of the acoustical stimulus and of the electrical stimulus was tested as well. The statistical significance level was set at 1 %.

3 Results

3.1 Acoustic stimulation

The synaptic current of inner hair cells was generated by a filtered homogeneous Poisson process as an acoustically stimulating one for 200 ms in time length at $I_{\text{amp}} = 3.0, 3.5, 4.0$, or 4.5 pA, $\lambda_c = 1000, 1500, 2000$, or 2500 s^{-1}, associated with sound pressure level, and $f = 220, 440$, or 880 Hz (See 4–6). The stimulating current was applied repeatedly 300 times to the peripheral end of ANF model, and then, the transmembrane potentials at the 36th node of Ranvier were recorded. The spike firing times were collected from 300 sample realizations to construct the post-stimulus time (PST) histogram.

The simulated synaptic current of inner hair cell, dot raster plot, and PST histogram is depicted for first 20 ms as a typical example for our regular conversation levels of 50–60 dB in SPL in the top, middle, and bottom row of Fig. 3, where $I_{\text{amp}} = 3.5$ pA, $\lambda_c = 2000\,\text{s}^{-1}$, and $f = 220$ Hz. The dots in the dot raster plot represent the spike firing occurrence times. The PST histogram generated from the spike firing occurrence times is drawn with a bin width of 0.2 ms in the bottom traces. It follows from Fig. 3 that the spike firing occurrence times or dot patterns are synchronized temporally to the occurrences of synaptic currents of inner hair cells, and the PST histograms can represent a periodicity of the underlying activity of inner hair cells.

The fundamental properties of the spike trains, i.e., the firing rates f_{spike} and the vector strength VS, as a function of the intensity of inner hair cell activity, λ_c, were investigated through Monte Carlo simulations. The von Mises parameters of X, κ, and μ were estimated by the maximum likelihood method according to Eqs. (12) and (13), and then, f_{spike} and VS were calculated on the basis of Eqs. (14) and (15). We

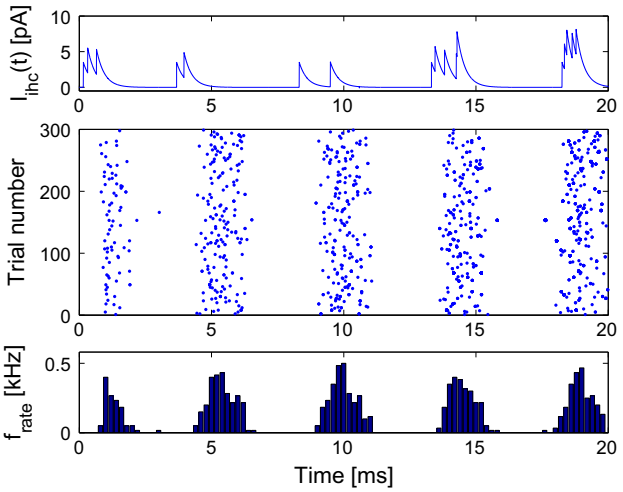

Fig. 3 Typical example of the acoustically stimulating current waveform of hair cell synapse (top), the dot raster plot (second row), and PST histogram (bottom) at $f = 220$ Hz, $I_{\text{amp}} = 3.5$ pA, and $\lambda_c = 2000\,\text{s}^{-1}$

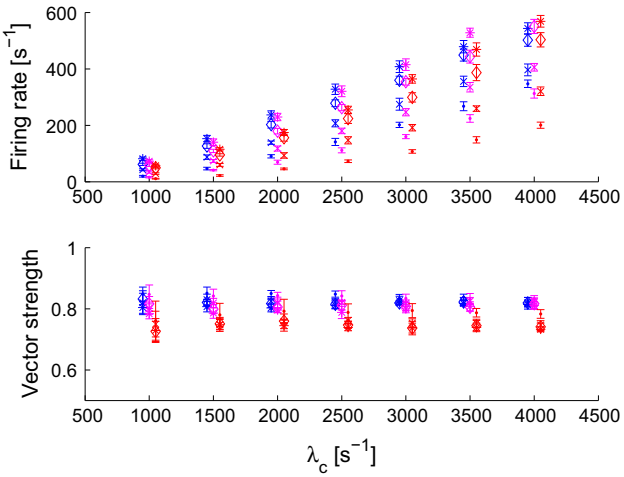

Fig. 4 The mean and standard deviation of $\hat{f}_{\text{spike}}$ (top) and $\hat{\text{VS}}$ (bottom) estimated from 10 Monte Carlo runs as a function of λ_c s^{-1} at an amplitude of the acoustic inner hair cell synaptic current, I_{amp}, of 3.0 (.), 3.5 (x), 4.0 (◊), 4.5 (*) at a frequency of 220 (blue), 440 (magenta), and 880 (red) Hz. Note that the statistics were corrected for removing neuron's refractory component via SEPP modeling (color figure online)

note that the estimated von Mises parameters are basically not influenced by neural refractory properties, since the spike trains are modeled by the one-memory SEPPs, which can represent the spike's aftereffects of reducing the intensity process. For Monte Carlo simulations, the parameter estimation was carried out repeatedly for 10 times, i.e., Monte Carlo runs = 10, and the mean and standard deviations of the estimated parameters were calculated. In Monte Carlo simulations, 10 sample realizations were gathered, i.e., P was set 10 in Eq. (13), a total time length of 2 s (200 ms $\times$ 10). Figure 4 shows the mean and standard deviation of $\hat{f}_{\text{spike}}$ (top)

and $\hat{\text{VS}}$ (bottom) estimated from 10 Monte Carlo runs as a function of $\lambda_c\ s^{-1}$ at an amplitude of the acoustic inner hair cell synaptic current, I_{amp}, of 3.0 (.), 3.5 (x), 4.0 (◊), 4.5 (*) at a frequency of 220 (blue), 440 (magenta), and 880 (red) Hz. We note that the statistics were corrected for removing neuron's refractory component via SEPP modeling. It suggests that the firing rates tend to increase as λ_c increases, depending upon the synaptic current amplitude, I_{amp}, and sinusoidal frequency f. The slopes of the firing rates as a function of λ_c tend toward greater at a greater value of I_{amp}, and tend toward smaller at a higher value of f. Meanwhile, the vector strength does not look a significant dependency of λ_c, taking a value of around 0.8.

3.2 Electric stimulation

The sinusoidally amplitude-modulated pulsatile waveform as a function of time for 200 ms at $I_p = 255, 260, 265$, or 270 μA, $m = 8$ to 24 %, and $f = 220, 440$, or 880 Hz was generated as an electrically stimulating current (See 7–9). The stimulating current was applied repeatedly 300 times to the electrode located at a distance of 1 mm above the second node of Ranvier of ANF model to obtain the spike firing occurrence times of the spike trains recorded at the 36th node of Ranvier.

The sinusoidally amplitude-modulated pulsatile electric stimuli, dot raster plot, and PST histogram are depicted for first 20 ms as a typical example in the top, middle, and bottom row of Fig. 5, where $I_p = 270$ μA, $m = 10$ %, and $f = 220$ Hz. The PST histogram generated from the spike firing occurrence times is drawn with a bin width of 0.2 ms. It follows from Fig. 5 that the spike firing occurrence times or dot patterns are synchronized temporally to the sinusoidal envelope of pulsatile electric stimuli, and the PST histograms can represent a periodicity of the sinusoidal signal, looking similar to that of acoustically stimulated situations shown in the bottom trace of Fig. 3.

The basic characteristics of the spike trains in response to pulsatile electric stimuli, f_{spike} and VS, as a function of the amplitude modulation depth, m, were investigated through Monte Carlo simulations. The von Mises parameters of X, κ, and μ were estimated by the maximum likelihood method according to Eqs. (12) and (13), and then, f_{spike} and VS were calculated on the basis of Eqs. (14) and (15). The parameter estimation was carried out repeatedly for 10 times, i.e., Monte Carlo runs = 10, and the mean and standard deviations of the estimated parameters were calculated. In Monte Carlo simulations, 10 sample realizations were gathered, i.e., P was set 10 in Eq. (13), a total time length of 2 s (200 ms × 10). Figure 6 shows the mean and standard deviation of $\hat{f}_{spike}$ (top) and $\hat{\text{VS}}$ (bottom) estimated from 10 Monte Carlo runs as a function of m at an amplitude of the unmodulated pulsatile

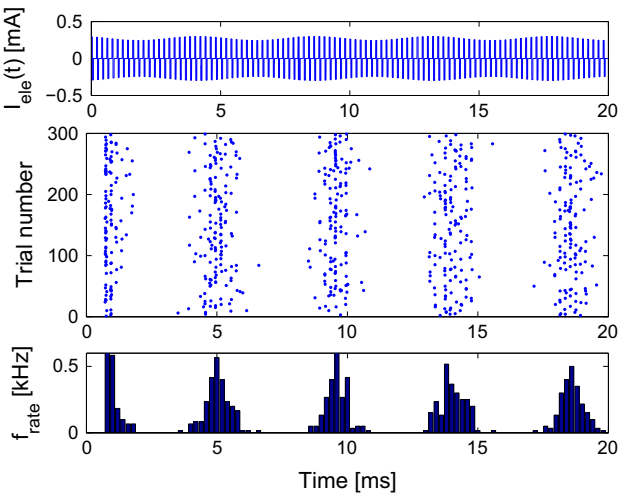

Fig. 5 Typical example of the electrically stimulating current waveform (top), the dot raster plot (second row), and PST histogram (bottom) at $f = 220$ Hz, $I_p = 270$ μA, and $m = 10$ %

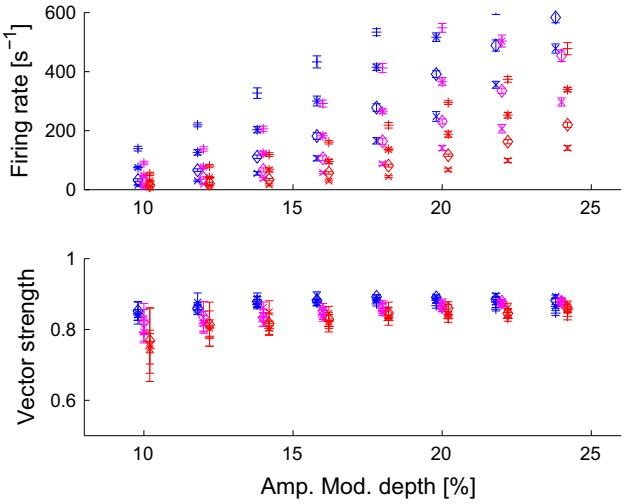

Fig. 6 The mean and standard deviation of $\hat{f}_{spike}$ (top) and $\hat{\text{VS}}$ (bottom) estimated from 10 Monte Carlo runs as a function of the amplitude modulation depth m % at an amplitude of the pulsatile waveform, I_{pulse}, of 255 (.), 260 (x), 265 (◊), 270 (*) at a frequency of 220 (blue), 440 (magenta), and 880 (red) Hz. Note that the statistics were corrected for removing neuron's refractory component via SEPP modeling (color figure online)

stimulating current, I_p, of 255 (.), 260 (x), 265 (◊), 270 (*) at a frequency of 220 (blue), 440 (magenta), and 880 (red) Hz. We note that the statistics were corrected for removing neuron's refractory component via SEPP modeling. The results of Monte Carlo simulations show that the firing rates tend to increase as m increases, depending upon the amplitude of unmodulated pulsatile stimuli, I_p, and sinusoidal frequency f. The slopes of the firing rates as a function of m tend toward greater at a greater value of I_p, and tend toward smaller at a higher value of f. In the mean time, the vector strength tends not toward a significant dependency of m, taking a value of

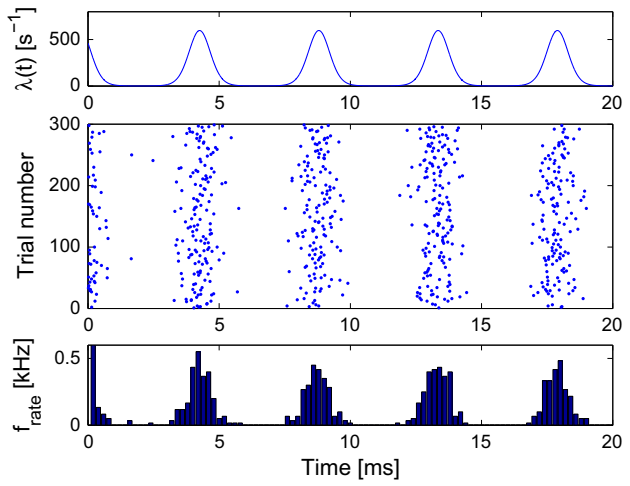

Fig. 7 Typical example of the periodic von Mises function without refractoriness (top), the dot raster plot of sample realizations of one-memory SEPPs artificially generated from random numbers (second row), and PST histogram (bottom) at $f = 220\,\text{Hz}$, $X = 23.843$, and $\kappa = 3.221$

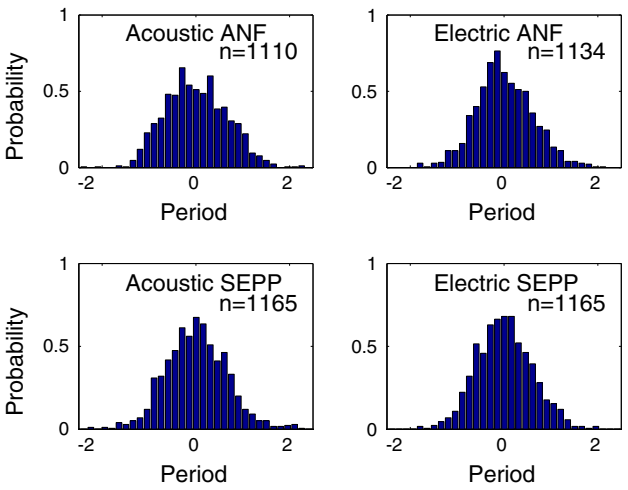

Fig. 8 The period histogram of the spike trains in response to acoustic stimulation at $I_{\text{amp}} = 3.5\,\text{pA}$, $\lambda_c = 2000\,\text{s}^{-1}$, and $f = 220\,\text{Hz}$ (top left), that of artificially generated one-memory SEPPs corresponding to acoustic situation at $X_{\text{ihc}} = 23.843$, $\kappa_{\text{ihc}} = 3.221$, and $f = 220\,\text{Hz}$ (bottom left), that of electrically stimulating ANFs at $I_p = 270\,\mu\text{A}$, $m = 10\,\%$, and $f = 220\,\text{Hz}$ (top right), and that of artificially generated one-memory SEPPs corresponding to electric situation at $X_{\text{ele}} = 17.535$, $\kappa_{\text{ele}} = 3.599$, and $f = 220\,\text{Hz}$ (bottom right). The number "n" in each inset indicates the number of angle data sampled from the spike firing times in which the total time length was set at 10 s. The bin width was set at 0.15

around 0.8. These results in electrically stimulated situations are similar to those of acoustically stimulated situations.

3.3 The uniform-scores test for acoustic or electric stimulus

The uniform-scores test was performed to quantitatively evaluate the equality of two period histograms, and further to assess the validity of modeling acoustically or electrically stimulated ANF spike trains with one-memory SEPPs of the von Mises type. A period histogram was generated from the spike firing times in response to acoustic stimulating currents (shown in the top trace of Fig. 3) or electric stimulating currents (shown in the top trace of Fig. 5), while another period histogram was created from the spike firing times of the artificially generated sample realizations of one-memory SEPPs of the von Mises type (see Fig. 7). The von Mises parameters of one-memory SEPPs corresponds to the mean of 10 parameters estimated from the spike trains in response to acoustic or electric stimulating currents on the basis of the maximum likelihood principle according to Eqs. (12) and (13).

Figure 8 depicts four kinds of period histograms: that of acoustically stimulated ANFs at $I_{\text{amp}} = 3.5\,\text{pA}$, $\lambda_c = 2000\,\text{s}^{-1}$, and $f = 220\,\text{Hz}$ (top left), that of artificially generated one-memory SEPPs of the von Mises type whose parameters correspond to the acoustically stimulated situation at $X_{\text{ihc}} = 23.843$, $\kappa_{\text{ihc}} = 3.221$, and $f = 220\,\text{Hz}$ (bottom left), that of electrically stimulated ANFs at $I_p = 270\,\mu\text{A}$, $m = 10\,\%$, and $f = 220\,\text{Hz}$ (top right), and that of artificially generated one-memory SEPPs of the von Mises type whose parameters correspond to the electrically stimulated situation at $X_{\text{ele}} = 17.535$, $\kappa_{\text{ele}} = 3.599$, and $f = 220\,\text{Hz}$ (bottom right).

The equality of two period histograms depicted at the top left and bottom left of Fig. 8 was assessed by the uniform-scores test at a statistical significance level of 1 %, suggesting that the acoustically stimulated ANF spike trains can be modeled by a one-memory SEPP of the von Mises type. The null hypotheses were not rejected for 3 typical situations of sound levels at $\lambda_c = 1500$, 2000, and $2500\,\text{s}^{-1}$ and at $f = 220$, 440, and 880 Hz.

The equality of two period histograms depicted at the top right and bottom right of Fig. 8 was assessed by the uniform-scores test at a statistical significance level of 1 %, suggesting that the electrically stimulated ANF spike trains can be modeled by a one-memory SEPP of the von Mises type. The null hypotheses were not rejected for 3 typical situations of sound levels at $m = 8$, 10, 12, 16, or $20\,\text{s}^{-1}$ and at $f = 220$, 440, and 880 Hz.

Furthermore, the equality of two period histograms of the acoustical stimulation at $I_{\text{amp}} = 3.5\,\text{pA}$, $\lambda_c = 2000\,\text{s}^{-1}$, and $f = 220\,\text{Hz}$ in the top left of Fig. 8 and of the electrical stimulation at $I_p = 270\,\mu\text{A}$, $m = 10\,\%$, and $f = 220\,\text{Hz}$ in the top right of Fig. 8 was validated by the uniform-scores test at a statistical significance level of 1 %. It follows from above that the parameters of an electric stimulating waveform, I_p, and m, can be optimally determined via one-memory SEPPs of the von Mises type in terms of matching two von Mises

parameters, $X_{\mathrm{ihc}} \approx X_{\mathrm{ele}}$ and $\kappa_{\mathrm{ihc}} \approx \kappa_{\mathrm{ele}}$ or matching two period histograms in response to acoustic and electric stimuli as a supplemental statistical evidence.

4 Discussions and conclusion

In the present paper, it has been shown that the spike trains of ANF models in response to acoustic stimuli of inner hair cells or amplitude-modulated pulsatile electric stimuli can be represented by one-memory SEPP of the von Mises type. The validity of modeling the spike trains in response to acoustic or electric stimuli with one-memory SEPPs of the von Mises type was assessed by the uniform-scores test using a comparison of two period histograms at a statistical significance level of 1 %. Furthermore, it is implied that an optimal electric stimulating waveform can be determined in terms of matching two von Mises parameters of acoustic and electric stimuli, i.e., $X_{\mathrm{ihc}} \approx X_{\mathrm{ele}}$ and $\kappa_{\mathrm{ihc}} \approx \kappa_{\mathrm{ele}}$, via one-memory SEPPs of the von Mises type, or matching two period histograms in response to acoustic and electric stimuli as a supplemental statistical evidence.

It is important for modeling spike trains to consider the refractory properties since the refractoriness makes it possible to distort the intensity process of random point process, and so reduce in a value of intensity processes, as is seen from Fig. 2. In the present study, a one-memory SEPP of the von Mises type has been adopted instead of inhomogeneous Poisson process (IHPP) of the von Mises type, because the estimation of the von Mises parameters by IHPP modeling gives us biased (incorrect) parameter values. That is, one-memory SEPPs with refractory properties can be expected to avoid biases of the estimated von Mises parameters due to distortion of intensity processes.

The fundamental characteristics of the spike trains, $\hat{f}_{\mathrm{spike}}$ and $\hat{\mathrm{VS}}$, corrected for removing refractory component, as a function of the intensity, λ_{c}, for acoustic stimulus and of the modulation depth, m, for electric stimulus were investigated as a first step. It was shown that the firing rates $\hat{f}_{\mathrm{spike}}$ monotonically increased as λ_{c} for acoustic stimulus or m for electric stimulus increased, while the vector strength $\hat{\mathrm{VS}}$ could not depend strongly on λ_{c} or m. It would be reasonable in statistical sense to determine an optimal electric stimulating waveform, directly from the observations of the fundamental characteristics between acoustic and electric stimuli. Also, it may be much more reasonable to do so, via the parameters of one-memory SEPPs, as the spike trains in response to acoustic or electric stimulus can be represented by one-memory SEPPs of the von Mises type.

Likewise, it is worth noting that an electric stimulating waveform can be determined so that the von Mises parameters of electric stimuli can be close or approximately equal to those of acoustic stimuli, i.e., $X_{\mathrm{ihc}} \approx X_{\mathrm{ele}}$ and $\kappa_{\mathrm{ihc}} \approx \kappa_{\mathrm{ele}}$, via one-memory SEPPs of the von Mises type, or the period histogram of the spike trains in response to electric stimuli can be equal to that in response to acoustic stimuli via one-memory SEPPs of the von Mises type. The step-by-step procedure of determining the electric stimulating parameters, i.e., pulse amplitude and modulation depth in our case, in terms of "matching von Mises parameters" may be as follows:

Step 1: Estimate the von Mises parameters, X_{ihc} and κ_{ihc}, from observation of the spike trains in response to acoustic stimuli within a parameter space of important speech cues, as is shown in Fig. 4.
Step 2: Estimate the von Mises parameters, X_{ele} and κ_{ele}, from observation of the spike trains in response to sinusoidally modulated pulsatile electric stimuli with an aid of the parameter values of X_{ihc} and κ_{ihc} without searching for a large-scale parameter space, as is shown in Fig. 6. We note an importance of SEPP modeling, as it would not only help remove refractory component, but also give us an insight into determining parameter spaces without thorough searching.
Step 3: Determine the electric stimulating parameters, pulse amplitude and modulation depth in our case, such that X_{ele} and κ_{ele} can be close or approximately equal to X_{ihc} and κ_{ihc}, i.e., $X_{\mathrm{ihc}} \approx X_{\mathrm{ele}}$ and $\kappa_{\mathrm{ihc}} \approx \kappa_{\mathrm{ele}}$, minimizing the mean squared error $[(X_{\mathrm{ihc}} - X_{\mathrm{ele}})^2 + (\kappa_{\mathrm{ihc}} - \kappa_{\mathrm{ele}})^2]/2$. To make sure the equality of von Mises parameters, the uniform-scores test was carried out as a supplemental statistical evidence on the basis of equality of two period histograms using two group angle data.

In the future, the concept presented in this paper would be useful for designing an optimal electric stimulating waveform on the basis of statistical principle and would be verified in animal experiments and/or clinical situations for cochlear implant users.

For low-rate pulsatile electric stimuli at 200–300 pps, an improvement of hearing performances has been found with low listening levels for several cochlear implant patients in clinical situations (Galvin and Fu 2005, 2009). In cases of lower pulse rates, one-memory SEPPs of the von Mises type would no longer be required for estimating the parameters without biasness, since the refractory properties might not distort the intensity processes. The IHPPs of the von Mises type, computationally more efficient and simpler than SEPPs, would be good enough for modeling the spike trains without considering the refractory properties, although one-memory SEPPs of the von Mises type would still be validated in cases of lower pulse rates. Even in cases of lower pulse rates, the concept verified in the present paper for a high

pulse rate of 5000 pps will work for determining an optimal electric stimulating waveform.

In this study, a conventional ANF model with a stochastic node of Ranvier was adopted, like that of (Imennov and Rubinstein 2009; Woo et al. 2009). Since the ANF model in the present paper would not consider adaptation or transient dynamics, extra ion channels like potassium channels with low threshold as well as cation channels and/or inner hair cell synaptic models with adaptation should be incorporated into the computational model, in cases of wide-sense stationarity unacceptable. In the present paper, we have focused on the temporal response properties of auditory nerve fiber model to a simple tone stimulus for a short time window of a hundred millisecond, in which an assumption of wide-sense stationarity would be validated, like that extensively accepted in speech processing and recognition. This is because it would be possible for transient dynamics to repeatedly make tracking of the von Mises parameters estimated from observations within a short time window as time advances. Also, we note that the sodium channels of Na v1.2 and/or v1.6 (Hossain et al. 2005; Hu et al. 2009) may make a change in spike initiations in ANFs. In the future, it shall be necessary to incorporate extra sodium ion channels into the node of Ranvier.

As a simple model for characterizing the spike trains in response to a single tone stimulus, one-memory SEPP of the von Mises type with a single sinusoidal function was adopted in the present work. We note that this approach would not be applicable for more complex aperiodic random processes without any modification. However, in principle, we may extend the intensity process consisting of a single tone sinusoidal function to multiple sinusoidal functions, like a Fourier series expansion, assuming that more "complicate" or "naturalistic" inputs could be expanded to a series of orthogonal functions. Or, we may do multivariate SEPPs in parallel fashion with specific frequency bands, like a cochlear filter bank.

In conclusion, the findings presented in this paper may play a key role in determining optimal parameters of pulsatile electric stimuli to efficiently encode information on important speech cues into the spike trains, and later in the design of better auditory neural prostheses.

Acknowledgements This work was supported by JSPS KAKENHI Grant Nos. 15K01397 and 18K10692.

References

Ashida G, Wagner H, Carr CE (2010) Processing of phase-locked spikes and periodic signals. In: Grun S, Rotter S (eds) Analysis parallel spike trains. Springer, New York, pp 59–74

Berry KJ II, Meister M (1998) Refractoriness and neural precision. J Neurosci 18:2200–2211

Bi Q (1989) A closed-form solution for removing the dead time effects from the poststimulus time histograms. J Acoust Soc Am 85:2504–2513

Carta JA, Bueno C, Ramírez P (2008) Statistical modelling of directional wind speeds using mixtures of von Mises distributions: case study. Energy Conver Manag 49:897–907

Cartee LA (2006) Spiral ganglion cell site of excitation ii: numerical model analysis. Hear Res 215:22–30

Clay JR, DeFelice LJ (1983) Relationship between membrane excitability and single channel open-close kinetics. Biophys J 42:151–157

Colburn HS, Carney LH, Heinz MG (2003) Quantifying the information in auditory-nerve responses for level discrimination. J Assoc Res Otolaryngol 4:294–311

Colombo J, Parkins CW (1987) A model of electrical excitation of the mammalian auditory-nerve neuron. Hear Res 31:287–312

Daley DJ, Vere-Jones D (2003) An introduction to the theory of point processes, 2nd edn. Springer, New York

Finley CC, Wilson BS, White MW (1990) Models of neural responsiveness to electrical stimulation. In: Miller JM, Spelman FA (eds) Cochlear implants: models of the electrically stimulated ear. Springer, New York, pp 55–96

Frijns JH, Mooij J, ten Kate JH (1994) A quantitative approach to modeling mammalian myelinated nerve fibers for electrical prosthesis design. IEEE Trans Biomed Eng 41:556–66

Galvin JJ, Fu Q-J (2005) Effects of stimulation rate, mode and level on modulation detection by cochlear implant users. J Assoc Res Otolaryngol 6:269–279

Galvin JJ, Fu Q-J (2009) Influence of stimulation rate and loudness growth on modulation detection and intensity discrimination in cochlear implant user. Hear Res 250:46–54

Gaumond RP, Molnar CE, Kim DO (1982) Stimulus and recovery dependence of cat cochlear nerve fiber spike discharge probability. J Neurophysiol 48:856–873

Gaumond RP, Kim DO, Molnar CE (1983) Response of cochlear nerve fibers to brief acoustic stimuli: role of discharge-history effects. J Acoust Soc Am 74:1392–1398

Goldberg JM, Brown PB (1969) Response of binaural neurons of dog superior olivary complex to dichotic tonal stimuli: some physiological mechanisms of sound localization. J Neurophysiol 32:613–636

Goldwyn JH, Shea-Brown E, Rubinstein JT (2010) Encoding and decoding amplitude-modulated cochlear implant stimuli—a point process analysis. J Comput Neurosci 28:405–424

Gray PR (1967) Conditional probability analyses of the spike activity of single neurons. Biophys J 7:759–777

Hawkes AG (1971a) Spectra and some self-exciting and mutually exciting point processes. Biometrika 58:83–90

Hawkes AG (1971b) Point spectra of some mutually exciting point processes. J R Stat Soc B 33:438–443

Heinz MG, Colburn HS, Carney LH (2001) Evaluating auditory performance limits: I. One-parameter discrimination using a computational model for the auditory nerve. Neural Comput 13:2273–2316

Hossain WA, Antic SD, Yang Y, Rasband MN, Morest DK (2005) Where is the spike generator of the cochlear nerve? Voltage-gated sodium channels in the mouse cochlea. J Neurosci 25:6857–6868

Hu W, Tian C, Li T, Yang M, Hou H, Shu Y (2009) Distinct contributions of Na v1.6 and Na v1.2 in action potential initiation and backpropagation. Nat Neurosci 12:996–1002

Imennov NS, Rubinstein JT (2009) Stochastic population model for electrical stimulation of the auditory nerve. IEEE Trans Biomed Eng 56:2493–2501

Johnson DH, Swami A (1983) The transmission of signals byauditory-nerve fiber discharge patterns. J Acoust Soc Am 74:493–501

Kumsa P, Mino H (2012) Effects of rates of spontaneous synaptic vesicle secretions in inner hair cells on information transmission in an auditory nerve fiber model. In: Proceedings of annual interna-

tional conference of the IEEE engineering in medicine and biology society, pp 2993–2996
Li J, Young ED (1993) Discharge-rate dependence of refractory behavior of cat auditory nerve fibers. Hear Res 69:151–162
Mardia KV, Jupp PE (1999) Directional statistics. Wiley, Chichester
Mark KE, Miller MI (1992) Bayesian model selection and minimum description length estimation of auditory-nerve discharge rates. J Acoust Soc Am 91:989–1002
Matsuoka AJ, Rubinstein JT, Abbas PJ, Miller CA (2001) The effects of interpulse interval on stochastic properties of electrical stimulation: models and measurements. IEEE Trans Biomed Eng 48:416–424
McDermott HJ (2004) Music perception with cochlear implants: a review. Trends Amplif 8:49–82
McNeal DR (1976) Analysis of a model for excitation of myelinated nerve. IEEE Trans Biomed Eng 23:329–337
Miller MI (1985) Algorithm for removing recovery related distortion from auditory-nerve discharge patterns. J Acoust Soc Am 77:1452–1464 with errata (1986), ibid, 570
Mino H (2001) Parameter estimation of the intensity process of self-exciting point processes using the EM algorithm. IEEE Trans Inst Meas 50:658–664
Mino H (2007) Encoding of information into neural spike trains in an auditory nerve fiber model with electric stimuli in the presence of a pseudospontaneous activity. IEEE Trans Biomed Eng 54:360–369
Mino H (2016) Modeling of the spike trains in response to sinusoidally amplitude-modulated pulsatile electric stimuli in auditory nerve fiber models with inhomogeneous poisson process of von mises type. Int J Bioelectromagn 18:2–7
Mino H, Rubinstein JT (2006) Effects of neural refractoriness on spatio-temporal variability in spike initiations with electrical stimulation. IEEE Trans Neural Syst Rehabil Eng 14:273–280
Mino H, Rubinstein JT, White JA (2002) Comparison of computational algorithms for the simulation of action potentials with stochastic sodium channels. Ann Biomed Eng 30:578–587
Mino H, Rubinstein JT, Miller CA, Abbas PJ (2004) Effects of electrode-to-fiber distance on temporal neural response with electrical stimulation. IEEE Trans Biomed Eng 51:13–20
Mouritsen H, Ritz T (2005) Magnetoreception and its use in bird navigation. Curr Opin Neurobiol 15:406–414
Neher E, Stevens CF (1977) Conductance fluctuations and ionic pores in membranes. Ann Rev Biophys Bioeng 6:345–381
Ogata Y (1981) On Lewis' simulation method for point processes. IEEE Trans Inf Theory IT–27:23–31
Ogata Y (1983) Likelihoodanalysis of point processes and its application to seismological data. Bull Int Stat Inst 2:954–961
Ogata Y, Katsura K (1986) Point-process models with linearly parametrized intensity for application to earthquake data. J Appl Prob 23:291–310
Ogata Y, Akaike H, Katsura K (1982) The application of linear intensity models to the investigation of causal relations between a point process and another stochastic process. Ann Inst Stat Math Part B 34:373–387
Ozaki T (1979) Maximum likelihood estimation of Hawkes' self-exciting point processes. Ann Inst Stat Math Part B 31:145–155
Papoulis A (1985) Probability, random variables, and stochastic processes, 2nd edn. McGraw-Hill, Singapore
Press WH, Teukolsky SA, Vetterling WT, Flannery BP (1993) Numerical recipes in C: the art of scientific computing. Cambridge University Press, New York, pp 847–851
Rubinstein JT (1995) Threshold fluctuations in an N sodium channel model of the node of Ranvier. Biophys J 68:779–785
Siebert WM (1965) Some implications of the stochastic behavior of primary auditory neurons. Kybernetik 2:206–215
Siebert WM (1970) Frequency discrimination in the auditory system: place or periodicity mechanisms? Proc IEEE 58:723–730
Siebert WM, Gray PR (1963) Random process model for the firing pattern of single auditory neurons. MIT QPR 71:241–245
Snyder DL, Miller MI (1991) Random point processes in time and space, 2nd edn. Springer, New York
Tejani VD, Abbas PJ, Brown CJ (2017) Relationship between peripheral and psychophysical measures of amplitude modulation detection in cochlear implant users. Ear Hear 38:e268–e284
van Hemmen JL (2013) Vector strength after Goldberg, Brown, and von Mises: biological and mathematical perspectives. Biol Cybern 107:385–396
van Hemmen JL, Longtin A, Vollmayr AN (2011) Testing resonating vector strength: auditory system, electric fish, and noise. Chaos 21:047508
Woo J, Miller CA, Abbas PJ (2009) Simulation of the electrically stimulated cochlear neuron: modeling adaptation to trains of electric pulses. IEEE Trans Biomed Eng 56:1348–1359